Acta Materialia 224 (2022) 117527

Contents lists available at ScienceDirect

Acta Materialia

journal homepage: www.elsevier.com/locate/actamat

Full length article

Disentangling diffusion heterogeneity in high-entropy alloys

Yi-Zhou Wang [a,b], Yun-Jiang Wang [a,b,*]

[a] State Key Laboratory of Nonlinear Mechanics, Institute of Mechanics, Chinese Academy of Sciences, Beijing 100190, China
[b] School of Engineering Science, University of Chinese Academy of Sciences, Beijing 101408, China

ARTICLE INFO

Article history:
Received 7 January 2021
Revised 28 October 2021
Accepted 26 November 2021
Available online 29 November 2021

Keywords:
Diffusion
Dynamic heterogeneity
High-entropy alloy
Molecular dynamics

ABSTRACT

Diffusion in the traditional single-crystalline solids is usually dynamically homogeneous characterized by a single-value or two characteristic activation energies. However, such a scenario breaks down at atomic-scale in the recently advanced high-entropy alloys, which are of unique structural features with multi-principal elements randomly occupying on lattice sites that induces strikingly local chemical heterogeneity. Here we uncover and decouple the possible dynamic heterogeneity accommodating the lattice diffusion in an archetypical high-entropy Cantor alloy CoCrFeMnNi via combined molecular statics, molecular dynamics, and a saddle-point sampling method. Wide distribution of vacancy formation energies and migration energies are revealed. We propose a single-vacancy and a vacancy-saturated model, respectively, to set up possible lower bound and upper bound of diffusivities. The models define a possible range of activation energies for the lattice diffusion in high-entropy alloys, which are comparable to experimental data. Finally, we argue that the conventional hypothesis of diffusion activation energy estimated from Arrhenius equation as the sum of the vacancy formation energy and migration energy becomes intractable in high-entropy alloys. These atomic-scale insights into diffusion heterogeneity, in contrast to the classical theory of homogeneous diffusion in conventional solid solutions, highlight the complexity of diffusion pathways and the intimate correlation between chemical, topological disorder and dynamic heterogeneity in the generic complex concentrated alloys.

1. Introduction

Diffusion is a basic mass transport mechanism in matters involving the motion of individual atom or collective atom groups at atomic scale [1]. Diffusion plays an important role in the phase stability and plastic deformation of materials, in particular, at a service condition of low stress and high temperature, e.g., the so-called creep deformation characterized by extremely low strain rate [2]. Thus, diffusion occupies a specific, yet significant, regime in the well-established Ashby deformation mechanism map of the crystalline solids [3].

In the conventional crystalline solids, e.g., metals and alloys, the diffusion mechanism has been well understood through atomic motion mechanisms either in the form of vacancy, or interstitial defect. The frequency of atomic motion is closely related to critical concept of diffusion coefficient, D, which measures how quick the diffusion event is. The diffusion coefficient is usually described in an empirical Arrhenius form

$$D(T) = fga^2\nu(T), \tag{1}$$

where f is a correlation factor considering the reversed atomic motion during diffusion, e.g., $f = 0.787$ in the conventional face-centered cubic (FCC) lattice [1], but becomes element specific in multi-component alloy [4,5]. g is a geometric factor of the order of unity in a cubic-symmetry lattice. a is the hopping distance of a diffusion defect along a possible diffusion path. And finally, ν is the frequency of the diffusion event which is temperature T and pressure dependent. In the framework of harmonic transition state theory (TST) [6], the frequency is depicted as

$$\nu(T) = \nu_0 \exp\left(\frac{\Delta S}{k_B}\right)\exp\left(-\frac{\Delta E}{k_B T}\right). \tag{2}$$

Here ν_0 is an attempt frequency of the order of atomic vibration ($\sim 10^{13}$ Hz). k_B is the Boltzmann's constant. ΔS is the activation entropy of diffusion due to the variation of vibrational state at saddle point, which is usually of a few k_Bs that is less relevant to diffusivity compared with the activation energy ΔE. The latter is usually up to several tens of $k_B T$s at ambient temperature, and therefore predominantly determines the magnitude of diffusivity. Note that the rate of a diffusion event is relevant to the Helmholtz free energy $\Delta F = \Delta E - T\Delta S$ via $D(T) \propto \exp(\frac{\Delta S}{k_B})\exp(-\frac{\Delta E}{k_B T})$ in the case of null pressure, according to Eq. (2). Therefore, only consideration of ΔE is incomplete in principle in the description of diffusion kinet-

* Corresponding author.
E-mail address: yjwang@imech.ac.cn (Y.-J. Wang).

https://doi.org/10.1016/j.actamat.2021.117527
1359-6454/

ics. There usually exists an empirically enthalpy-entropy compensation which indicates proportionality between ΔS and ΔE, even in high-entropy alloy [7]. This correlation brings out a complex scenario in diffusion kinetics, i.e., diffusivity is not purely determined by activation energy, but it is a combined function of activation energy (or enthalpy of diffusion without existence of pressure) and the pre-exponential factor. The latter is a function of activation entropy ΔS. On the one hand, a larger activation energy gives lower diffusivity according to Eq. (2). On the other hand, larger activation energy is usually correlated with larger activation entropy, which will increase the diffusion kinetics, on the contrary. Consequently, activation energy is sometimes misleading because the slow-moving element can also exhibit lower activation energy by simultaneously exhibiting the lower value of pre-exponential factor because of $D(T) = f(\Delta E, \Delta S)$.

The traditional understanding of diffusion in solids mostly relies on ΔE, which is usually a definite single-value parameter within a finite temperate range if the atomic-scale mechanism is invariant. For example, $\Delta E = 2.0$ eV quantifies the kinetics of vacancy diffusion mechanism in bulk single-crystalline copper. To clarify a specific plastic mechanism, if one measures the activation energy of this order of magnitude, from either experiment or computer simulation, it can be postulated empirically that the atomic-scale plastic mechanism is lattice diffusion. In comparison, if one has the knowledge of a much smaller activation energy of $\Delta E \sim 0.6$ eV in copper [8], it is presumably to be grain boundary diffusion, which is treated as a short-circuit diffusion path in polycrystals. Note that sometimes it is necessary to have multiple distinct activation energies due to the appearance of different diffusion mechanisms and, therefore, leading to the non-Arrhenius like behavior of diffusion. One known example of a pure element is iron, which presents a curvature of the temperature dependence of lattice diffusion at the transition temperature of the different magnetic states [9]. Other examples are alloys like TiAl [10] or NiAl [11] materials with hcp crystalline structure. Very recently, it becomes aware that a non-Arrhenius temperature dependence of lattice diffusion of the constituent elements in a prototypical multicomponent alloy [5]. As a result, it is urgent to understand the atomic-scale mechanism of diffusion heterogeneity in complex concentrated alloy.

However, such a conventional scenario of diffusion with a multiple distinct activation energies become intractable in a category of new metals, i.e., the recently emerging and greatly advanced multi-principal-element, or complex concentrated, or mostly dynamically termed high-entropy alloys (HEAs) [12–19]. In the high-entropy alloys, there are usually more than five principal elements that occupy randomly on a specific lattice site, e.g., FCC or BCC, which inevitably brings about chemical and structural heterogeneity at nanoscale in the alloys [20,21]. On the one hand, high-resolution transmission electron microscopy has observed pronounced local chemical order (LCO) in several medium-, or high-entropy alloys [22–27]. The LCO induces either strengthening or softening effect in the complex metals and extreme multiplicity of dislocation pathways [23,24,26]. On the other hand, computer simulations of both atomic- and electronic-scale have revealed a wide spectrum of stacking fault energies and Peierls stresses in a specific high-entropy alloy [21,28], which is in strong contrast with conventional solid solutions with one unique value of a physical quantities. All the information points to a unique structural feature of the generic high-entropy alloy, namely, the atomic-scale heterogeneity in terms of both topology and dynamics [29]. However, the latter has rarely been touched in literature, due to the extreme challenge of an in situ observation of dynamic process with atomic-scale resolution [26], especially in the case of diffusion which involves participation of only one or several atoms.

One the most intriguing phenomenon is the so-called sluggish diffusion which is deemed as one of the major high-entropic effects in HEAs [30,31], although the concept is still controversial [4,32,33]. The nominal random distribution of elements on lattice site actually induces inhomogeneous lattice distortion locally [34,35], which sometimes yields a sluggish diffusion mechanism in the complexly distorted lattice field owing to the strain or stress incompatibility [36–42]. Then a question naturally arises whether the conventional scenario of diffusion obtained from usual metals and alloys stands robustly in the high-entropy alloys. At least, in analogy to stacking fault energy, the activation energy of diffusion should not be a single-value parameter, due to existence of the short-range structural heterogeneity [5,7,43]. Experimentalists have used interdiffusion technique and/or direct radiotracer diffusion measurement to study the mass transport mechanism in both lattice (bulk) and grain boundary of high-entropy alloys [4,5,7,44–48]. However, the understanding is still of a mean-field sense, with a typical single-value activation energy. Such works indeed capture a key feature of large activation energy of lattice diffusion of the order of 3–4 eV, which is corresponding to the sluggish diffusion with low diffusion coefficient. Since a phenomenon of non-Arrhenius diffusion has been clearly noticed in the quinary high-entropy Cantor alloy [5], it is interesting to understand the microscopic mechanism and quantify the diffusion heterogeneity in HEAs. Recent atomistic simulations and Monte Carlo modellings of diffusion in multi-principal-element alloys shed light on settling this issue [4,21,28,43].

To exploit atomic-scale mechanism, in particular, the dynamic heterogeneity of diffusion in HEAs, we perform molecular dynamics (MD) simulations to investigate the diffusion mechanism of a model Cantor alloy, i.e., the five-component equiatomic CoCrFeMnNi alloy, that has been extensively studied as a benchmark system in the community. The diffusion heterogeneity will be expressed as a wide range of vacancy formation energies and migration energies in the case of lattice diffusion. Handshake with the experimental mean-field physical parameters is discussed. The dynamic heterogeneity adds new knowledge to the theory of diffusion in solids, which is expected to be generalized for the generic complex concentrated alloys.

2. Methodology

2.1. Atomic model and molecular dynamics

An equimolar five-component high-entropy Cantor alloy, CoCrFeMnNi, is used in the MD simulations as a model of the general multi-principal-element alloys. The atomic structure is shown in Fig. 1(a). A full random occupation of lattice site is considered, thus generating a high-entropy alloy of the ideal mixing configurational entropy (upper bound of entropy). The single-crystalline model is of FCC, which contains approximately 100 000 atoms, with designed dimensions of $107.85 \times 107.85 \times 107.85$ Å^3. Note that the present random model does not account for the concept, e.g., role of enthalpy of mixing in clustering or heterogeneity. Therefore, proper development of chemical short-range order or phase separation is suppressed. The role of structural ordering in diffusion dynamic of HEA deserves further study.

The atomic interaction in the model is described by a second nearest-neighbor modified embedded-atom method (MEAM) potential [43]. This empirical potential gives rise to a list of reasonable physical properties that enables it to be widely used to study the diffusion behavior and mechanical deformation of the present CoCrFeMnNi alloy. Especially the alloying effect was testified well for the critical resolved shear stress. The deformation twinning phenomenon at cryogenic temperature was also reproduced by this potential [43]. The sluggish diffusion phenomenon was also rationalized by the appearance of stable vacant lattice sites with large migration energy as trap positions. Finally, after stress relaxation

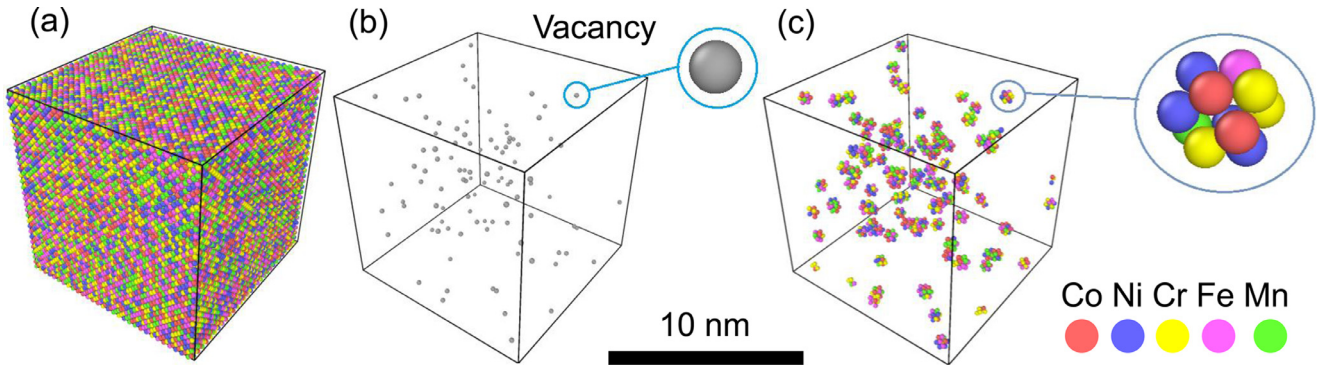

Fig. 1. Atomic model of the Cantor alloy. (a) Visualization of the atomic configuration of the CoCrFeMnNi alloy. (b) Generating 100 vacancies in the model by randomly removing 100 atoms, with each component 20 atoms, respectively. The shown vacancies are recognized by Wigner-Seitz defect analysis. (c) Visualization of the vacancies by their 12 nearest neighbor atoms. Red, blue, yellow, pink and green balls represent Co, Ni, Cr, Fe and Mn atoms, respectively. The scale bar is 10 nm.

and energy minimization, the potential yields lattice parameter of 3.595 Å, which is in agreement with experimental value 3.59 [49].

In order to observe the lattice diffusion mechanism, we remove a fraction of atoms to make lattice vacancies. For a first approximation, the equilibrium vacancy concentration (0.1%) at the melting temperature is introduced [50]. As such it is reasonable to randomly remove 100 atoms (20 for each element) from the perfect FCC lattice (with 100 000 atoms), which generates a vacancy-saturated model at relatively lower temperature than the melting point. However, this operation gives to an upper limit of the lattice diffusivity, which is in contrast with the one-vacancy model that sets the lower bound for diffusivity. To speed up diffusion, we adopt a smaller model with about 10 000 atoms in order to notice pronounced diffusion behavior with finite MD time window, e.g., 10 ns. Then an experimental diffusivity should between the results of the two models – the vacancy-saturated and one-vacancy model. Then we use a conjugate gradient algorithm to energetically minimize the position of atoms in the vacancy-saturated model. The vacancy-saturated model is further shown in Figs. 1(b) and 1(c), with clear visualization of the random positions of vacancies, after removing the perfect FCC atoms for clarity. Atomic visualization is performed by OVITO software [51]. The vacancies are identified by the Wigner-Seitz cell method in Fig. 1(b) and the common neighbor analysis [52] in Fig. 1(c).

For the MD simulations of diffusion, we adopt a canonical ensemble with periodic boundary conditions in the three directions. The time step for integration of Newtonian equation of motion in MD is 2 fs. The temperature and pressure are controlled by the Nosé–Hoover thermostat [53,54]. The diffusion is observed via atomic motion at a temperature range between 1300 K and 1600 K, with interval of 50 K. Note that the melting point of this MEAM potential for Cantor alloy is calculated to be 1910 K by MD, which is much higher than that of the experimental data 1607 K. In order to make the simulations relevant to experimental studies of diffusion, we restrict the MD simulations of diffusion at temperature below 1600 K. Before tracing the mean-squared displacement (MSD), the model is heated to a targeted temperature with a reasonable duration of thermal equilibration.

2.2. Minimum energy pathway of vacancy diffusion

The possible minimum migration energies of a vacancies are exhaustively explored with the activation-relaxation technique nouveau (ARTn) [55–57]. ARTn is a kind of generic approach to study the thermally activated local structural excitations involving rearrangement of atoms which are usually rare events for atomistic simulations. Compared with the classical MD, it can deal with simulations on a much longer timescale that is relevant to the experimental conditions [58,59]. An ART event is defined as a hopping process from a local energy minimum to the neighboring minimum, after crossing a potential energy barrier on the potential energy landscape [60,61]. Here the diffusion pathway is along 12 possible directions guided by the nearest-neighbor positions of a vacancy along the ⟨111⟩ crystallographic direction [62]. Starting with a specific vacancy, the initial perturbation with amplitude of 0.05 Å is performed on the vacancy's 12 nearest neighbors by setting an affected cutoff distance of 2.5 Å (separating the nearest and 2nd nearest neighbors). The initial direction of displacement is random, thus, guarantee a thorough exploration of reaction pathways. After which, the configuration is dragged along the weakest direction of the high-dimensional Hessian space until the curvature of the investigated pathway is smaller than -0.30 eV/Å^2. Then the configuration is pushed to the saddle point by the Lanczos algorithm. Finally, the vacancy is relaxed to a neighboring position after energy minimization. The migration energy is thereafter defined as the energy difference between the saddle configuration and initial energy minimum state. Activation of each atom for 10 times and therefore there are altogether 11 990 migration events in the vacancy-saturated model. Since the chemical environment of each vacancy is unique, there is anticipated to be a reasonable range of migration energies for each element.

3. Results

3.1. Atomic-scale dynamic heterogeneity from trajectories

To gain a preliminary insight into the diffusion heterogeneity in high-entropy alloy, we trace the trajectories of each type of element in both the one-vacancy and vacancy-saturated model after running canonical MD for 10 ns at 1600 K. For this purpose, we select a slice of atoms normal to z : [001] direction for visualization. Therefore, it is an operation of projection of 3D diffusion pattern on the xy plane. The trajectories of atoms are shown in Fig. 2. In the case of one-vacancy model, most of the atoms are vibrating around their equilibrium positions as shown in Fig. 2(a). A few atoms, in particular the Mn and Co ones, have escaped from their initial positions, travelling some proper distance which indicates diffusion happens during the 10 ns MD time. In the case of vacancy-saturated model, a significant fraction of the atoms has experienced diffusion events via migration of random vacancies. It is expected that the pattern shown in Fig. 2(a) will become alike that of Fig. (b) if time is long enough to allow the single vacancy travel across the whole sample. The most intriguing feature of the observation is that there exists strongly difference in the hopping distances of different elements. It is obvious that Mn and Co atoms diffuse longer distance than the other elements. It means

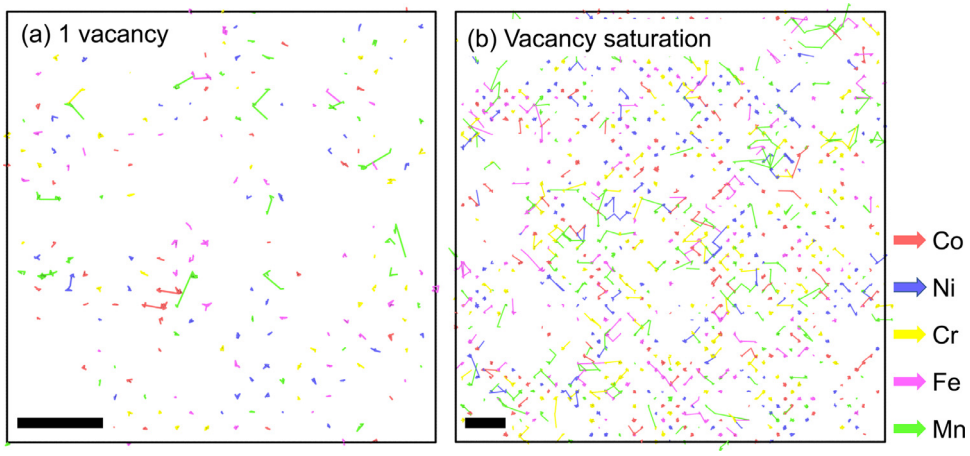

Fig. 2. Diffusion heterogeneity illustrated by the trajectories of atoms during a canonical MD simulation for 1 ns. (a) Atomic model with one vacancy, and (b) vacancy saturation model with 100 random vacancies, respectively. The shown slice is of 107.85 Å thickness along the z : [001] direction. A scale bar of 1 nm is shown in the left bottom corner of each panel.

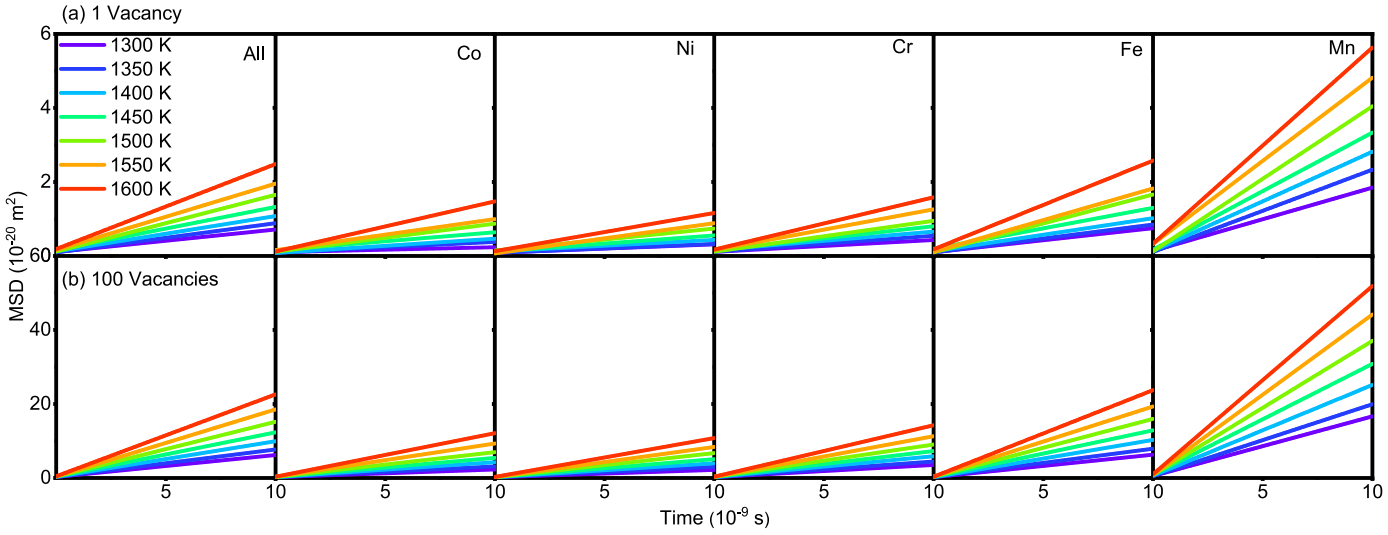

Fig. 3. Mean-squared displacement of all atoms and each type of atom in the (a) one vacancy, and (b) vacancy-saturated model, which set up lower and upper bound of diffusivities, respectively. The apparent diffusivities are estimated from the slopes of these curves by linear fit according to Eq. (3).

that these atoms are dynamically more active than the rest, which will be argued quantitatively later with activation energy of the thermal activation event. As a result, Fig. 2 intuitively demonstrates the dynamic heterogeneity of lattice diffusion in high-entropy alloy, in sharp contrast with the scenario of homogeneous lattice diffusion in conventional metals and alloys.

3.2. Define a possible regime of diffusivity

To quantitatively characterize the dynamic heterogeneity, we turn to the physical parameters that are relevant to lattice diffusion – diffusion coefficient and activation energy – which can be extracted from the Arrhenius relationship used to depict the thermally activated material processes. Fig. 3 shows the MSD–time relationship curves of all atoms, and the specific category of atoms, at different temperatures. The testing temperature range is between 1300 and 1600 K, which is below the experimental melting point 1607 K. The interval of observation temperature is 50 K. For the MD duration of 10 ns, the MSDs have established linear relationship with time. The faster the MSD curve rises, the easier the atoms diffuse. It is obvious that the MSDs in the vacancy-saturated model are much bigger than those of the one-vacancy model, which is in accord with the diffusion patterns shown in Fig. 2. In both upper and lower panel, the MSDs of Mn atoms rise with the fastest speed amongst the five elements, while the MSDs of Ni rise the slowest. It indicates Mn is more active than Ni, which is also in agreement with the observation of trajectories shown in Fig. 2. Furthermore, MSDs increase faster with increasing temperature, especially at 1600 K. This trend is straightforward since diffusion is a thermally activated process which is accelerated by rising temperature.

The apparent MD diffusivity $D^*(T)$ of each element at temperature T are calculated according to the Einstein relation by taking derivative of MSD with respect to time, i.e.

$$D^*(T) = \frac{\langle |\mathbf{r}(\tau) - \mathbf{r}(0)|^2 \rangle}{6\tau}, \tag{3}$$

where $\mathbf{r}(\tau)$ and $\mathbf{r}(0)$ are the position vectors of atoms. $\tau = 10$ ns is the time duration of MD for tracing diffusion. The angle brackets stand for ensemble average. Therefore, the fitting data of the curves' slopes in Fig. 3 yield the corresponding apparent diffusivities. The one-vacancy and vacancy-saturated model produce lower bound of diffusion D_{lower}, and upper bound D_{upper}, respectively, for the lattice diffusion in the present high-entropy alloy.

According to thermodynamics of materials, the equilibrium concentration of vacancy is temperature-dependent, i.e., $C(T) =$

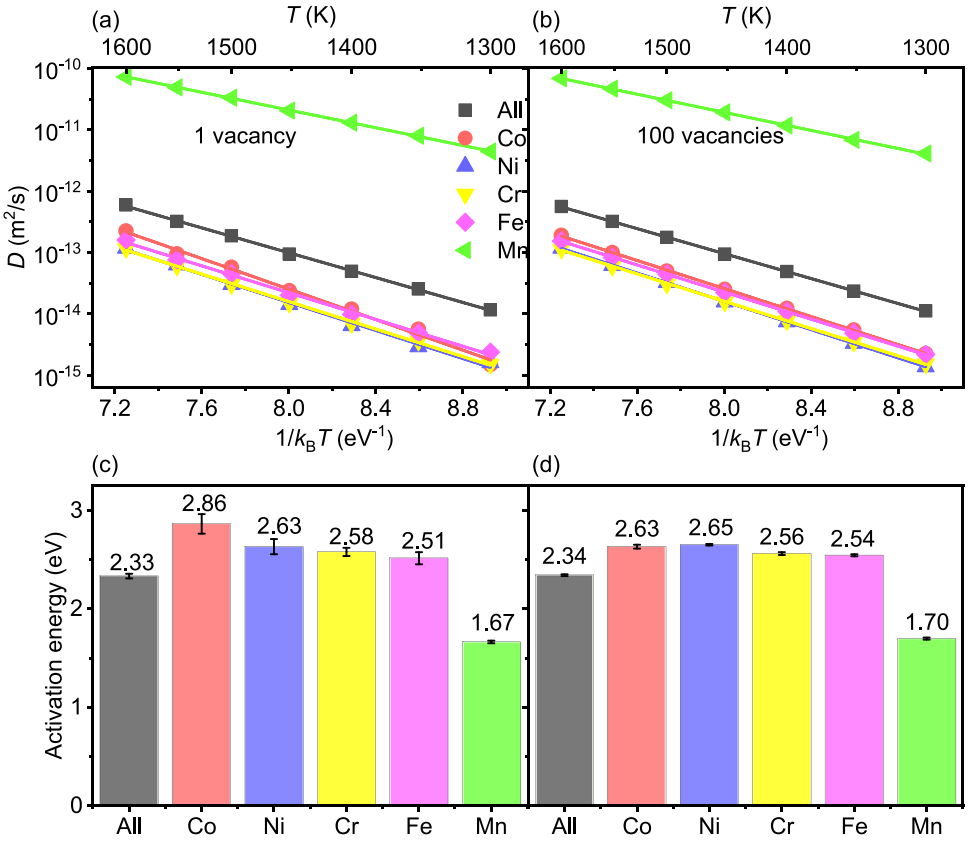

Fig. 4. Arrhenius plot of diffusivities of different type of atoms in the (a) one vacancy, and (b) vacancy-saturated model, respectively. The effective activation energies of each type of atom are displayed in (c) for one vacancy, and in (d) for vacancy-saturated model, respectively. The error bars in (c) and (d) denote uncertainty in Arrhenius fits shown in (a) and (b).

$\exp(-E_f/k_BT)$. However, the translation from MD calculated apparent diffusivity $D^*(T)$ to a physical diffusivity $D(T)$ is not intuitive, especially with the appearance of multiple equivalent elements in HEAs. In the present work, the equilibrium concentration of vacancy of the ith element is determined after Ref. [63], which reads

$$C_i(T) = \frac{\exp\left(n - 1 - \frac{E_f^i}{k_BT}\right)}{n + \exp\left(n - 1 - \frac{E_f^i}{k_BT}\right)}. \quad (4)$$

Here E_f^i is the average value of the vacancy formation energy of the ith element, which will be calculated statistically in Fig. 5. n is the total number of elements in a HEA. Then the physical and apparent diffusivities can be connected through $\frac{D(T)}{D^*(T)} = \frac{C(T)}{C^*(\mathrm{MD})}$ at any specific temperature. While $D^*(T)$ and $C(T)$ can be calculated via Eqs. (3) and (4), the equilibrium concentration of vacancy in the MD model, i.e., $C^*(\mathrm{MD})$, has been set up to be approximately 10^{-4} and 10^{-3} in the one-vacancy, and the vacancy-saturated model, respectively.

The corresponding effective activation energies – mean-field sense single-value parameters – for the lower bound $\Delta E_{\mathrm{lower}}$ and upper bound $\Delta E_{\mathrm{upper}}$ are both calculated according to the Arrhenius equation [combing Eqs. (1) and (2)] via

$$\Delta E = -\frac{\partial \ln D(T)}{\partial (1/k_BT)}. \quad (5)$$

Note that the lower bound activation energy $\Delta E_{\mathrm{lower}}$ corresponds to the upper bound of diffusivity in the vacancy-saturated model and vice versa.

The Arrhenius plot of the physical diffusivities against reciprocal temperature are shown in Fig. 4 for the two models. After translation from MD simulations to real case, the effective magnitude of diffusivity of all atoms in Cantor alloy is of the order of 10^{-14} m^2/s at 1300 K, which is a reasonable value in analogy with the experimental data of $\sim 10^{-15}$ m^2/s [5,7]. Furthermore, the reported diffusivities shown in Figs. 4(a) and (b) are of similar magnitudes in both the one-vacancy and vacancy-saturated model, which illustrates the validity of the two models in predicting diffusion dynamics of HEA from atomistic simulations. At any temperature in both cases, the diffusion coefficient of Mn is of the largest value, while the other four elements are of similar diffusivities. The diffusivity of all atoms in a mean-field sense is in between the two groups. Finally, all the data lie well on the Arrhenius law prediction, indicating a well-defined activation energy for each element.

In Figs. 4(c) and (d) we show the histograms of the mean-field sense activation energies for each element, along with the effective value for the whole model. In the latter case, the types of atoms are not distinguished in both the one-vacancy and vacancy-saturated model, respectively. The upper bound of activation energies in Fig. 4(c) is almost identical to that of the lower bound in the vacancy-saturated model as shown in Fig. 4(d), except the case of Co which shows a difference of 0.2 eV. The lower and upper bounds together define a regime of possible activation energies of diffusion in the real high-entropy sample, which can be benchmarked by the activation energy from experiments, e.g., from the isotope tracer technique for diffusion. For example, the activation energy of Co diffusion was estimated to be 2.80 eV in Cantor alloy [4,7], which lies well in the regime of activation energies defined here, e.g., 2.63–2.86 eV from simulations. However, we note that the real number of activation energy has close relation with the accuracy of the interatomic potential adopted in MD.

While the purpose of the present simulations and modellings is to provide some basic idea on the atomic-scale mechanism of diffusion as well as the qualitative trend, it does capture the feature of distinct diffusion parameters for different elements. The conclusion is argued by the histogram of activation energies shown in Figs. 4(c) and (d). It is evidence of dynamic heterogeneity of the lattice diffusion in random complex alloy, i.e., the barrier is element specific. In both of the one-vacancy and vacancy-saturated atomic models, Mn has been shown to be of the lowest activation energy which indicates it is the most active atom in the alloy. This finding is consistent with previous MD calculations with the same MEAM potential [43]. It is also in agreement with kinetic Monte Carlo simulations which have found Mn is of the lowest energy barrier among others [4]. The small activation energy of Mn is also evidenced by the longer hopping distance in Fig. 2. Ni, Cr and Fe seem to present similar dynamics of diffusion in the alloy. This observation is also consistent with experimental observation [7]. However, the behavior of Co is a bit obscure. While Co has a similar value of activation energy to Ni, Cr, and Fe in the vacancy-saturated model, it is of the largest activation energy in the one-vacancy model, signifying the complexity of the atomic-scale dynamic behavior of atoms in the complex alloy.

In sum, the MD simulations using MEAM potential renders an order of Mn >> Co ≈ Fe > Cr ≈ Ni about diffusivity in CoCrFeMnNi alloy at 1300 K, which is in qualitative agreement with radiotracer measurement in Ref. [7], which provided an order of Mn >> Cr > Fe > Ni >> Co at the same temperature. In terms of activation energy in the surveyed temperature range, the atomistic simulations suggest an order of Co > Ni > Cr > Fe >> Mn in the one vacancy model and Ni ≈ Co > Cr ≈ Fe >> Mn in the vacancy saturated model. However, in experiment, the activation energies are found to be in the order (Co ≈ Mn) > (Fe ≈ Ni) > Cr [7]. This discrepancy in diffusivity and activation energy implies the significant role of activation entropy, i.e., the diversity in activation pathways under thermal fluctuation, plays an important role in diffusion kinetics of high-entropy alloys. Note that MEAM empirical potential in general overestimates diffusivity and underestimates activation energy. Therefore, it is not capable of quantitatively simulating diffusion in the present HEA.

3.3. Disentangling the dynamic heterogeneity of diffusion

The conventional rationalization of diffusion activation energy arises from two aspects. One is the vacancy formation energy which determines the concentration of defect at thermodynamic equilibrium, and the other is the vacancy migration energy which levels the difficulty of thermal excitation, with the two steps constituting a complete description of the diffusion dynamics. Following this strategy, here we begin with calculating the vacancy formation energy of any atom belonging to a specific element in the high-entropy alloy according to

$$E_f = E_v - \frac{N-1}{N} E_{bulk}. \quad (6)$$

Here E_v represents the potential energy of the model with one vacancy after removing an atom (after energy minimization), and E_{bulk} denotes the energy of the perfect lattice. N is the number of atoms in the perfect lattice and, thus, E_{bulk}/N represents the potential energy of the removed atom, i.e., the chemical potential μ. Due to the fact that there are five kinds of elements in the present alloy, we use the average value of the potential energy of each type of atom as a reference value for the chemical potential. Since LCO exists in the complex alloys, the formation energy of any element is expected to be of an appropriate distribution instead of a unique value.

The postulation of the appearance of reasonable distribution of formation energy of vacancy is evidenced in Fig. 5(a), which reports the spectra for each element. The distributions mostly lie in a range of 1.2–2 eV, this is in agreement with experimental value of 1.69 ± 0.13 eV by positron lifetime measurements [64]. Among them, Mn is of the smallest formation energy of vacancy, which is consistent with the fact that it moves fastest, as demonstrated in Figs. 2–4. As anticipated, there are distinct distribution of formation energies around the most probable value, with energy domain spanning up to sub-eV scale. This feature applies to any constituent element of the HEA. The distribution of the vacancy formation energy signifies the atomic-scale structural heterogeneity and the associated spatially heterogeneous bonding feature in complex alloy. In light of the full width at half maximum (FWHM) of the distribution, one might judge the heterogeneity of vacancy formation energy sorts in an order of Mn (0.45) > Fe (0.34) > Co (0.32) > Cr (0.29) > Ni (0.24). Here the numbers in parentheses (in unit of eV) represent FWHM of the GaussAmp fits in Fig. 5(a). However, it will be shown later that such heterogeneity in vacancy formation energy is less than the heterogeneity in migration energy. Moreover, the existence of the high formation energy vacant sites (up to 2 eV) is critical for the sluggish diffusion, since such sites are thermodynamically stable and might hinder the thermally activated motion of vacancy. Consequently, the LCO may postpone diffusion and slow down global dynamics of the metastable HEA.

In comparison to formation energy, the migration energy of diffusion presents wider distribution and therefore enhances dynamic heterogeneity of diffusion. Here we use ARTn to search for the possible migration energies of a vacancy for each type of atom along the initial random directions. Then it is converged to one of the minimum energy migration pathways along the nearest-neighbor directions of an FCC lattice, i.e., the ⟨111⟩ crystallographic directions. Note that the migration of a vacancy actually corresponds to the opposite movement of a nearest-neighboring atom. Therefore, the migration energy can be assigned to a specific type of element. The explored histogram of migration energies E_m for all the atoms of each type are displayed in the lower panels of Fig. 5. In contrast with the spectra of vacancy formation energies, the migration energies distribute with a much wider range, spanning a scope of approximately 2 eV that is more than twice of that of formation energies. One therefore may claim that the dynamic heterogeneity of lattice diffusion in complex concentrated alloys is mainly driven by the heterogeneity of migration energy rather than the formation energy. In a quantitative manner, the sequence of dynamic heterogeneity in migration energy is Co (1.00) > Cr (0.94) > Ni (0.87) > Mn (0.57) > Fe (0.50), here again the numbers in parentheses (in eV) denote FWHM of distributions in Fig. 5(b). Furthermore, the mean migration energies of these elements are of the order of 0.5–0.6 eV, which are in quantitative agreement with both MD and nudged elastic band method calculations based on the same empirical potential [4,43].

The shaped areas in each panel of Fig. 5 denote a possible range of activation energies, which are defined by the lower and upper bound of activation energies from the vacancy-saturated, and one-vacancy model, respectively. The dashed vertical lines are the reported experimental values of activation energies for each element in CoCrFeMnNi alloy from Ref. [7]. It is found that the MD estimated activation energy of Co is in agreement quantitively with experimental data. However, the MD underestimates the activation energies for the rest four elements. The discrepancy is possibly from the lack of quantitative accuracy of the MEAM potential, since the present simulations echo well with previous MD and kMC simulations [4,43] using the same potential. However, all the simulations produce higher diffusivity than experiments. Therefore, the next generation energetic representation such as machine-learning neural network interatomic potential is necessitated to deal with quantitative simulations of dynamics in random alloy with quantum-level accuracy [65]. Finally, except the distri-

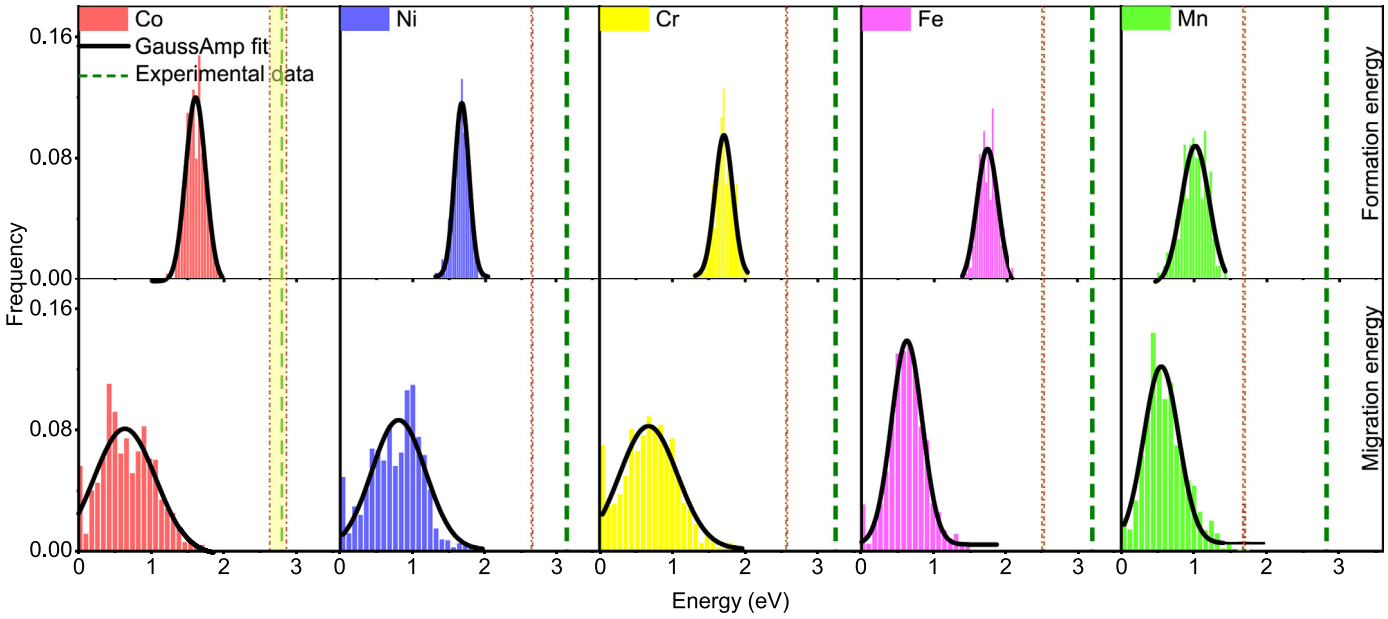

Fig. 5. Spectra of vacancy formation energy (upper panel) and migration energy (lower panel) for each element in the vacancy-saturated model. The curve in each panel represents a best nonlinear fit according to the amplitude Gaussian peak function. The yellow shape areas between dash dot lines denotes the MD-estimated range of activation energy, defined by diffusivity of the lower bound (one vacancy) and upper bound (vacancy-saturation), respectively. The vertical lines indicate the values of the experimental activation energies for each element.

bution in activation energies, we note that the pre-exponential factor D_0 also depends on activation entropy of diffusion and the correlation factor. The latter is not the same for all the constituting elements in the CoCrFeMnNi high-entropy alloy [5], which is also a source of possible diffusion heterogeneity in the generic multi-principal element alloys.

4. Discussion

In the conventional metals and alloys with only one or two principal elements, the diffusion kinetics is well understood through a single-value, or multiple distinct activation energies. For a fixed lattice diffusion mechanism with a unique value of activation energy, its value is assumed the sum of the formation energy and migration energy of a vacancy, i.e., $\Delta E = E_f + E_m$. However, the striking feature of diffusion in complex concentrated alloys is the dynamic heterogeneity featured by a wide distribution of the formation energies and migration energies. Therefore, the circumstance becomes intractable in such alloys since it is not straightforward anymore to define a physically sound effective formation energy and migration energy for a specific constituting element. To probe into a possible scenario of diffusion kinetics in high-entropy alloys, we plot the sum $(E_f + E_m)$ as a function of real value of activation energy from the direct Arrhenius fit. The results are shown in Fig. 6 for both of the two models investigated with the vacancy-saturated and one-vacancy conditions. Here E_f and E_m are both statistical average value of their distributions as shown in Fig. 5. The experimental activation energies for the elements in the alloy with the same composition are also provided in Fig. 6 to calibrate the MD calculations.

There are several intriguing features about lattice diffusion in high-entropy alloys which can be noticed from Fig. 6. First, the activation energies of diffusion for the constituting element are different. It is evidence of the chemical heterogeneity in HEA that can be intuitively understood. Next, judged from a first approximation $\Delta E_{mean} = (\Delta E_{lower} + \Delta E_{upper})/2$ from the two MD models, shown as open squares in Fig. 6, the mean activation energies fall into the range of 1.70–2.80 eV, which is smaller than the experimental

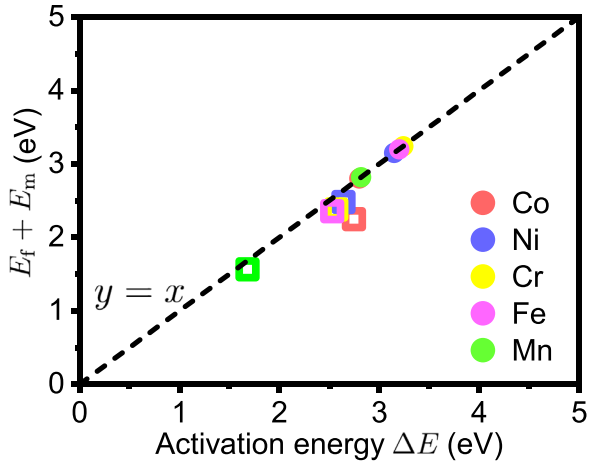

Fig. 6. The relationship between the MD estimated activation energy ΔE of diffusion, the experimental activation energy and the sum of the mean value of vacancy formation and migration energy from MD simulations, respectively. The black line $y = x$ denotes usual understanding of $\Delta E = E_m + E_f$. The open squares stand for the mean values of the lower (ΔE_{lower}) and upper bound (ΔE_{upper}) of activation energies in the vacancy-saturated and one-vacancy model, respectively. The experimental activation energies of elements are shown by solid circles on the $y = x$ line.

data of 2.80–3.24 eV. The disagreement is possibly attributed to a couple of reasons, e.g., inaccuracy of the empirical potential, the difference in testing temperature range of simulations and experiments, and the oversimplification of the formation energy and the migration energy as an average value of the wide distribution, etc. However, the MD simulations does provide qualitative feature of diffusion kinetics in Cantor alloy, e.g., Mn moves fastest among the five constituents. The modellings from the two distinct models do provide reasonable understanding of diffusion heterogeneity in the category of high-entropy alloys. It decouples the atomic-scale dynamic heterogeneity from a physical perspective in a quantitative manner. Then, if one further examines the MD data, the usual assumption of thermodynamics $\Delta E = E_m + E_f$ breaks down quantita-

tively although the data are near the dashed line. Exactly speaking, the simple rule predicts data below the $y = x$ line and therefore will definitely underestimate activation energies. Finally, a physically sound and sophisticated model considering both the nature of spatial heterogeneity and the rugged diffusion potential energy landscape is furthermore required to fully disentangling the diffusion heterogeneity of HEAs.

5. Conclusion

In sum, a one-vacancy and a vacancy-saturated model of the quinary Cantor alloy is proposed as a prototype to study the general dynamic heterogeneity of lattice diffusion in high-entropy alloys via atomistic simulations described by an empirical MEAM potential. The models set up upper bound and lower bound of diffusivities, respectively, which renders a possible range of activation energies that is qualitatively comparable to the experimental data. Further molecular statics calculations about the formation energies of vacancy and exhaustive exploration of possible migration energies clearly demonstrate the pronounced distributions in the spectra of both vacancy formation energy and vacancy migration energy. Therefore, the dynamic heterogeneity is physically decoupled with atomic-scale information about each type of component. The distribution of the vacancy migration energies is twice wider than that of the formation energies which suggests the former as the major contribution to the diffusion heterogeneity. Therefore, we initiate a new scenario about the diffusion heterogeneity in the recently emerging complex concentrated alloy that is in sharp contrast with the scenario of a single-value activation energy or multiple distinct ones in the conventional elemental metals and solid solutions.

The findings also challenge the view of activation energy of diffusion as a sum of vacancy formation energy and migration energy. Such a simple approximation will underestimate the activation energy as the present simulations informed. Thus, more sophisticated model is necessitated to rationalize the diffusion heterogeneity in HEAs by taking account the topological feature of chemically heterogeneity and roughness of potential energy landscape. Consequently, the present insights into diffusion of the complex concentrated alloys shed light on connecting the structural and dynamic heterogeneity of generic multi-principal-element alloys. The information is heuristic for the constitutive modellings of mechanics of HEAs which should take into account the strikingly distribution of physical parameters attributed to the atomic-scale structural heterogeneity. Finally, empirical interatomic potential with quantum accuracy via machine learning huge configurational and chemical space is anticipated to enable quantitative prediction of diffusion behaviors in the generic medium- or high-entropy alloys and other solids.

Declaration of Competing Interest

The authors declare that they have no known competing financial interests or personal relationships that could have appeared to influence the work reported in this paper.

Acknowledgement

This work is financially supported by the National Natural Science Foundation of China (under grant No. 12072344), and the Youth Innovation Promotion Association of the Chinese Academy of Sciences (under Grant No. 2017025). The numerical calculations were performed on the CAS Xiandao-1 computing environment.

References

[1] H. Mehrer, Diffusion in solids: fundamentals, methods, materials, Diffusion-Controlled Processes, Springer, Berlin, Heidelberg, Berlin, 2007, doi:10.1007/978-3-540-71488-0.
[2] M.E. Kassner, Fundamentals of Creep in Metals and Alloys, Elsevier Ltd., Amsterdam, 2008 Second ed, doi:10.1016/B978-0-08-047561-5.X0001-2.
[3] M.F. Ashby, A first report on deformation-mechanism maps, Acta Metall 20 (1972) 887–897, doi:10.1016/0001-6160(72)90082-X.
[4] J. Kottke, D. Utt, M. Laurent-Brocq, A. Fareed, D. Gaertner, L. Perrière, Ł. Rogal, A. Stukowski, K. Albe, S.V. Divinski, G. Wilde, Experimental and theoretical study of tracer diffusion in a series of (CoCrFeMn)100−xNix alloys, Acta Mater 194 (2020) 236–248, doi:10.1016/j.actamat.2020.05.037.
[5] D. Gaertner, J. Kottke, Y. Chumlyakov, F. Hergemöller, G. Wilde, S.V. Divinski, Tracer diffusion in single crystalline CoCrFeNi and CoCrFeMnNi high-entropy alloys: kinetic hints towards a low-temperature phase instability of the solid-solution? Scr. Mater. 187 (2020) 57–62, doi:10.1016/j.scriptamat.2020.05.060.
[6] H. Eyring, The Activated Complex in Chemical Reactions, J. Chem. Phys. 3 (1935) 107, doi:10.1063/1.1749604.
[7] M. Vaidya, K.G. Pradeep, B.S. Murty, G. Wilde, S.V. Divinski, Bulk tracer diffusion in CoCrFeNi and CoCrFeMnNi high entropy alloys, Acta Mater 146 (2018) 211–224, doi:10.1016/j.actamat.2017.12.052.
[8] M. Sørensen, Y. Mishin, A.F. Voter, Diffusion mechanisms in Cu grain boundaries, Phys. Rev. B. 62 (2000) 3658–3673, doi:10.1103/PhysRevB.62.3658.
[9] F.S. Buffington, K. Hirano, M. Cohen, Self diffusion in iron, Acta Metall 9 (1961) 434–439, doi:10.1016/0001-6160(61)90137-7.
[10] S.V. Divinski, F. Hisker, T. Wilger, M. Friesel, C. Herzig, Tracer diffusion of boron in α-Ti and γ-TiAl, Intermetallics 16 (2008) 148–155, doi:10.1016/j.intermet.2007.08.008.
[11] S.V. Divinski, C. Herzig, On the six-jump cycle mechanism of self-diffusion in NiAl, Intermetallics 8 (2000) 1357–1368, doi:10.1016/S0966-9795(00)00062-5.
[12] J.-W. Yeh, S.-K. Chen, S.-J. Lin, J.-Y. Gan, T.-S. Chin, T.-T. Shun, C.-H. Tsau, S.-Y. Chang, Nanostructured High-Entropy Alloys with Multiple Principal Elements: novel Alloy Design Concepts and Outcomes, Adv. Eng. Mater. 6 (2004) 299–303, doi:10.1002/adem.200300567.
[13] B. Cantor, I.T.H. Chang, P. Knight, A.J.B. Vincent, Microstructural development in equiatomic multicomponent alloys, Mater. Sci. Eng. A. 375–377 (2004) 213–218, doi:10.1016/j.msea.2003.10.257.
[14] E.P. George, D. Raabe, R.O. Ritchie, High-entropy alloys, Nat. Rev. Mater. 4 (2019) 515–534, doi:10.1038/s41578-019-0121-4.
[15] Y.F. Ye, Q. Wang, J. Lu, C.T. Liu, Y. Yang, High-entropy alloy: challenges and prospects, Mater. Today. 19 (2016) 349–362, doi:10.1016/j.mattod.2015.11.026.
[16] Z. Li, S. Zhao, R.O. Ritchie, M.A. Meyers, Mechanical properties of high-entropy alloys with emphasis on face-centered cubic alloys, Prog. Mater. Sci. 102 (2018) 296–345, doi:10.1016/J.PMATSCI.2018.12.003.
[17] B. Gludovatz, A. Hohenwarter, D. Catoor, E.H. Chang, E.P. George, R.O. Ritchie, A fracture-resistant high-entropy alloy for cryogenic applications, Science 345 (2014) 1153–1158, doi:10.1126/science.1254581.
[18] Z. Li, K.G. Pradeep, Y. Deng, D. Raabe, C.C. Tasan, Metastable high-entropy dual-phase alloys overcome the strength–ductility trade-off, Nature (2016), doi:10.1038/nature17981.
[19] D. Raabe, C.C. Tasan, E.A. Olivetti, Strategies for improving the sustainability of structural metals, Nature 575 (2019) 64–74, doi:10.1038/s41586-019-1702-5.
[20] E. Ma, Unusual dislocation behavior in high-entropy alloys, Scr. Mater. 181 (2020) 127–133, doi:10.1016/j.scriptamat.2020.02.021.
[21] Q.-J. Li, H. Sheng, E. Ma, Strengthening in multi-principal element alloys with local-chemical-order roughened dislocation pathways, Nat. Commun. 10 (2019) 3563, doi:10.1038/s41467-019-11464-7.
[22] Z. Zhang, M.M. Mao, J. Wang, B. Gludovatz, Z. Zhang, S.X. Mao, E.P. George, Q. Yu, R.O. Ritchie, Nanoscale origins of the damage tolerance of the high-entropy alloy CrMnFeCoNi, Nat. Commun. 6 (2015) 10143, doi:10.1038/ncomms10143.
[23] Q. Ding, Y. Zhang, X. Chen, X. Fu, D. Chen, S. Chen, L. Gu, F. Wei, H. Bei, Y. Gao, M. Wen, J. Li, Z. Zhang, T. Zhu, R.O. Ritchie, Q. Yu, Tuning element distribution, structure and properties by composition in high-entropy alloys, Nature 574 (2019) 223–227, doi:10.1038/s41586-019-1617-1.
[24] R. Zhang, S. Zhao, J. Ding, Y. Chong, T. Jia, C. Ophus, M. Asta, R.O. Ritchie, A.M. Minor, Short-range order and its impact on the CrCoNi medium-entropy alloy, Nature 581 (2020) 283–287, doi:10.1038/s41586-020-2275-z.
[25] R. Zhang, S. Zhao, C. Ophus, Y. Deng, S.J. Vachhani, B. Ozdol, R. Traylor, K.C. Bustillo, J.W. Morris, D.C. Chrzan, M. Asta, A.M. Minor, Direct imaging of short-range order and its impact on deformation in Ti-6Al, Sci. Adv. 5 (2019), doi:10.1126/sciadv.aax2799.
[26] F. Wang, G.H. Balbus, S. Xu, Y. Su, J. Shin, P.F. Rottmann, K.E. Knipling, J.-C. Stinville, L.H. Mills, O.N. Senkov, I.J. Beyerlein, T.M. Pollock, D.S. Gianola, Multiplicity of dislocation pathways in a refractory multiprincipal element alloy, Science 370 (2020) 95–101, doi:10.1126/science.aba3722.
[27] X. Chen, Q. Wang, Z. Cheng, M. Zhu, H. Zhou, P. Jiang, L. Zhou, Q. Xue, F. Yuan, J. Zhu, X. Wu, E. Ma, Direct observation of chemical short-range order in a medium-entropy alloy, Nature 592 (2021) 712–716, doi:10.1038/s41586-021-03428-z.
[28] J. Ding, Q. Yu, M. Asta, R.O. Ritchie, Tunable stacking fault energies by tailoring local chemical order in CrCoNi medium-entropy alloys, Proc. Natl. Acad. Sci. U. S. A. 115 (2018) 8919–8924, doi:10.1073/pnas.1808660115.
[29] F.-H. Cao, Y.-J. Wang, L.-H. Dai, Novel atomic-scale mechanism of incipient plasticity in a chemically complex CrCoNi medium-entropy alloy associated

with inhomogeneity in local chemical environment, Acta Mater 194 (2020) 283–294, doi:10.1016/j.actamat.2020.05.042.
[30] Y. Zhang, T.T. Zuo, Z. Tang, M.C. Gao, K.A. Dahmen, P.K. Liaw, Z.P. Lu, Microstructures and properties of high-entropy alloys, Prog. Mater. Sci. 61 (2014) 1–93, doi:10.1016/j.pmatsci.2013.10.001.
[31] K.Y. Tsai, M.H. Tsai, J.W. Yeh, Sluggish diffusion in Co-Cr-Fe-Mn-Ni high-entropy alloys, Acta Mater 61 (2013) 4887–4897, doi:10.1016/j.actamat.2013.04.058.
[32] Y.N. Osetsky, L.K. Béland, A.V. Barashev, Y. Zhang, On the existence and origin of sluggish diffusion in chemically disordered concentrated alloys, Curr. Opin. Solid State Mater. Sci. 22 (2018) 65–74, doi:10.1016/j.cossms.2018.05.003.
[33] M.S. Daw, M. Chandross, Sluggish diffusion in random equimolar FCC alloys, Phys. Rev. Mater. 5 (2021) 043603, doi:10.1103/PhysRevMaterials.5.043603.
[34] Y.F. Ye, Y.H. Zhang, Q.F. He, Y. Zhuang, S. Wang, S.Q. Shi, A. Hu, J. Fan, Y. Yang, Atomic-scale distorted lattice in chemically disordered equimolar complex alloys, Acta Mater 150 (2018) 182–194, doi:10.1016/j.actamat.2018.03.008.
[35] H. Song, F. Tian, Q. Hu, L. Vitos, Y. Wang, J. Shen, N. Chen, Local lattice distortion in high-entropy alloys, Phys. Rev. Mater. 1 (2017) 023404, doi:10.1103/PhysRevMaterials.1.023404.
[36] J. Dąbrowa, M. Danielewski, State-of-the-Art Diffusion Studies in the High Entropy Alloys, Metals (Basel) 10 (2020) 347, doi:10.3390/met10030347.
[37] S.V. Divinski, A.V. Pokoev, N. Esakkiraja, A. Paul, A Mystery of "Sluggish Diffusion" in High-Entropy Alloys: the Truth or a Myth? Diffus. Found. 17 (2018) 69–104, doi:10.4028/www.scientific.net/DF.17.69.
[38] J. Kottke, M. Laurent-Brocq, A. Fareed, D. Gaertner, L. Perrière, Ł. Rogal, S.V. Divinski, G. Wilde, Tracer diffusion in the Ni–CoCrFeMn system: transition from a dilute solid solution to a high entropy alloy, Scr. Mater. 159 (2019) 94–98, doi:10.1016/j.scriptamat.2018.09.011.
[39] A. Mehta, Y. Sohn, Investigation of sluggish diffusion in FCC Al0.25CoCrFeNi high-entropy alloy, Mater. Res. Lett. 9 (2021) 239–246, doi:10.1080/21663831.2021.1878475.
[40] A. Mehta, Y. Sohn, High Entropy and Sluggish Diffusion "Core" Effects in Senary FCC Al–Co–Cr–Fe–Ni–Mn Alloys, ACS Comb. Sci. 22 (2020) 757–767, doi:10.1021/acscombsci.0c00096.
[41] A. Mehta, Y. Sohn, Interdiffusion, Solubility Limit, and Role of Entropy in FCC Al-Co-Cr-Fe-Ni Alloys, Metall. Mater. Trans. A. 51 (2020) 3142–3153, doi:10.1007/s11661-020-05742-z.
[42] V. Verma, A. Tripathi, K.N. Kulkarni, On interdiffusion in FeNiCoCrMn high entropy alloy, J. Phase Equilibria Diffus. 38 (2017) 445–456, doi:10.1007/s11669-017-0579-y.
[43] W.-M. Choi, Y.H. Jo, S.S. Sohn, S. Lee, B.-J. Lee, Understanding the physical metallurgy of the CoCrFeMnNi high-entropy alloy: an atomistic simulation study, Npj Comput. Mater. 4 (2018) 1, doi:10.1038/s41524-017-0060-9.
[44] M. Vaidya, S. Sen, X. Zhang, L. Frommeyer, Ł. Rogal, S. Sankaran, B. Grabowski, G. Wilde, S.V. Divinski, Phenomenon of ultra-fast tracer diffusion of Co in HCP high entropy alloys, Acta Mater 196 (2020) 220–230, doi:10.1016/j.actamat.2020.06.025.
[45] M. Glienke, M. Vaidya, K. Gururaj, L. Daum, B. Tas, L. Rogal, K.G. Pradeep, G. Wilde, S.V. Divinski, Grain boundary diffusion in CoCrFeMnNi high entropy alloy: kinetic hints towards a phase decomposition, Acta Mater (2020), doi:10.1016/j.actamat.2020.05.009.
[46] D. Gaertner, K. Abrahams, J. Kottke, V.A. Esin, I. Steinbach, G. Wilde, S.V. Divinski, Concentration-dependent atomic mobilities in FCC CoCrFeMnNi high-entropy alloys, Acta Mater 166 (2019) 357–370, doi:10.1016/j.actamat.2018.12.033.
[47] J. Zhang, G.M. Muralikrishna, A. Asabre, Y. Kalchev, J. Müller, B. Butz, S. Hilke, H. Rösner, G. Laplanche, S.V. Divinski, G. Wilde, Tracer diffusion in the σ phase of the CoCrFeMnNi system, Acta Mater 203 (2021) 116498, doi:10.1016/j.actamat.2020.116498.
[48] M. Vaidya, S. Trubel, B.S. Murty, G. Wilde, S.V. Divinski, Ni tracer diffusion in CoCrFeNi and CoCrFeMnNi high entropy alloys, J. Alloys Compd. 688 (2016) 994–1001, doi:10.1016/j.jallcom.2016.07.239.
[49] P.P. Bhattacharjee, G.D. Sathiaraj, M. Zaid, J.R. Gatti, C. Lee, C.W. Tsai, J.W. Yeh, Microstructure and texture evolution during annealing of equiatomic CoCrFeMnNi high-entropy alloy, J. Alloys Compd. 587 (2014) 544–552, doi:10.1016/j.jallcom.2013.10.237.
[50] W. Cai, W.D. Nix, Imperfections in Crystalline Solids, Cambridge University Press, 2016, doi:10.1017/CBO9781316389508.
[51] A. Stukowski, Visualization and analysis of atomistic simulation data with OVITO-the Open Visualization Tool, Model. Simul. Mater. Sci. Eng. 18 (2010) 015012, doi:10.1088/0965-0393/18/1/015012.
[52] J.D. Honeycutt, H.C. Andemen, Molecular Dynamics Study of Melting and Freezing of Small Lennard-Jones Clusters, J. Phys. Chem. 91 (1987) 4950–4963, doi:10.1021/j100303a014.
[53] Nosé Shūichi, A molecular dynamics method for simulations in the canonical ensemble, Mol. Phys. 52 (1984) 255–268, doi:10.1080/00268978400101201.
[54] W.G. Hoover, Canonical dynamics: equilibrium phase-space distributions, Phys. Rev. A. 31 (1985) 1695–1697, doi:10.1103/PhysRevA.31.1695.
[55] G.T. Barkema, N. Mousseau, Event-Based Relaxation of Continuous Disordered Systems, Phys. Rev. Lett. 77 (1996) 4358, doi:10.1103/PhysRevLett.77.4358.
[56] R. Malek, N. Mousseau, Dynamics of lennard-jones clusters: a characterization of the activation-relaxation technique, Phys. Rev. E. 62 (2000) 7723, doi:10.1103/PhysRevE.62.7723.
[57] E. MacHado-Charry, L.K. Béland, D. Caliste, L. Genovese, T. Deutsch, N. Mousseau, P. Pochet, Optimized energy landscape exploration using the ab initio based activation-relaxation technique, J. Chem. Phys. 135 (2011) 034102, doi:10.1063/1.3609924.
[58] D. Rodney, C. Schuh, Distribution of Thermally Activated Plastic Events in a Flowing Glass, Phys. Rev. Lett. 102 (2009) 235503, doi:10.1103/PhysRevLett.102.235503.
[59] D. Rodney, A. Tanguy, D. Vandembroucq, Modeling the mechanics of amorphous solids at different length scale and time scale, Model. Simul. Mater. Sci. Eng. 19 (2011) 083001, doi:10.1088/0965-0393/19/8/083001.
[60] F.H. Stillinger, Energy Landscapes, Inherent Structures, and Condensed-Matter Phenomena, Princeton University Press, 2016, doi:10.2307/j.ctvc77g0v.
[61] D. Wales, Energy Landscapes: Applications to Clusters, Biomolecules and Glasses, Cambridge University Press, 2004, doi:10.1017/CBO9780511721724.
[62] J. Du, W.-T. Geng, K. Arakawa, J. Li, S. Ogata, Hydrogen-Enhanced Vacancy Diffusion in Metals, J. Phys. Chem. Lett. 11 (2020) 7015–7020, doi:10.1021/acs.jpclett.0c01798.
[63] Z. Wang, C.T. Liu, P. Dou, Thermodynamics of vacancies and clusters in high-entropy alloys, Phys. Rev. Mater. 1 (2017) 043601, doi:10.1103/PhysRevMaterials.1.043601.
[64] K. Sugita, N. Matsuoka, M. Mizuno, H. Araki, Vacancy formation enthalpy in CoCrFeMnNi high-entropy alloy, Scr. Mater. 176 (2020) 32–35, doi:10.1016/j.scriptamat.2019.09.033.
[65] Y. Mishin, Machine-learning interatomic potentials for materials science, Acta Mater 214 (2021) 116980, doi:10.1016/j.actamat.2021.116980.